mathematics

MDPI

Article

A New Prestress Loss Calculation Model of Anchor Cable in Pile–Anchor Structure

Xing Gao [1], Jinqing Jia [1,*], Guoxiong Mei [2], Xiaohua Bao [3], Lihua Zhang [1] and Xiaoping Liao [4]

[1] The State Key Laboratory of Coastal and Offshore Engineering, Dalian University of Technology, Dalian 116024, China; gao_x@mail.dlut.edu.cn (X.G.); lihua2018@dlut.edu.cn (L.Z.)
[2] College of Civil Engineering and Architecture, Guangxi University, Nanning 530004, China; meiguox@163.com
[3] School of Civil and Transportation Engineering, Shenzhen University, Shenzhen 518061, China; bxh@szu.edu.cn
[4] Northwest Research Institute Co., Ltd. of China Railway Engineering Corporation, Lanzhou 730000, China; xiaoping.liao@126.com
* Correspondence: jiajq@dlut.edu.cn

Abstract: Pile–anchor structures are widely used in foundation excavation and slope reinforcement due to their safety and reliability. However, the pile–anchor structures have the common problem of the prestress loss of anchor cables, which may reduce the stability of the structures. To accurately predict the prestress loss of anchor cables, a new prestress loss calculation model was established, and the availability of the prestress loss calculation model was verified through engineering cases. Meanwhile, aiming at the long-term prestress loss of anchor cables, the coupled creep behavior of anchor cable–rock and soil was studied and an anchor cable–rock and soil coupled creep model suitable for pile–anchor structures is proposed. The model test confirms that the coupled creep model could accurately describe the coupled creep behavior of the anchor cable and the rock and soil mass. The models provide a theoretical basis for the study of the prestress of anchor cables in pile–anchor structures, and have a guiding significance for the design and construction in foundation excavation and slope engineering.

Keywords: pile–anchor structure; coupled creep model; prestress loss; prestressed anchor cable; model test; field test

MSC: 74F99

Citation: Gao, X.; Jia, J.; Mei, G.; Bao, X.; Zhang, L.; Liao, X. A New Prestress Loss Calculation Model of Anchor Cable in Pile–Anchor Structure. *Mathematics* **2022**, *10*, 1260. https://doi.org/10.3390/math10081260

Academic Editor: Nikolai A. Kudryashov

Received: 7 March 2022
Accepted: 8 April 2022
Published: 11 April 2022

1. Introduction

In recent years, pile–anchor structures have been widely used in foundation excavation, slope reinforcement, and other support engineering, which have the characteristics of high reliability, short period, and low cost. The principle of the pile–anchor support system is to maintain the stability of the slope through the anchoring force provided by anchor cables and the anti-sliding force provided by anti-sliding piles. Nowadays, the research on pile–anchor structures has mainly focused on the soil characteristics, seismic effects, and pile length effects [1–5]. Scholars have mostly focused on the special problem of the structures and ignored the common problem, that is, the prestress loss of anchor cables. Therefore, it is extremely important to establish a calculation model for pile–anchor structures that can predict the prestress loss of anchor cables in actual projects.

The prestress loss of anchor cables can be divided into instantaneous loss and long-term loss. Many scholars have conducted long-term prestress monitoring of anchor cables through field and model tests, confirming the objective existence of the long-term loss and proposed prediction models [6–8]. Nowadays, most of the prediction models are empirical models that can accurately predict the prestress loss of anchor cables in similar projects, but they are not suitable for every project [9–13]. Based on this, mechanical creep models have been proposed, whose constituent elements have clear physical meaning, and model parameters can be obtained from creep tests [14–18]. However, the current coupled creep models only consider the mechanical properties of the anchor cable and the rock and soil mass, and ignore the influence of external factors. Due to the existence of anti-slide piles in pile–anchor structures, the coupling mode of the anchor cable and the rock and soil mass changes. Therefore, an anchor cable–rock and soil coupled creep model and a prestress loss calculation model suitable for pile–anchor structures were established.

Nowadays, in the study of material creep properties, the fractional derivative methods and the integer derivative methods have evolved as the two most effective methods of describing the characteristics of viscoelastic materials. The advantage of fractional derivative methods is that the viscoelastic behavior can be accurately described by fewer parameters [19–21]. However, the fractional derivative methods have certain drawbacks, and the computational cost and memory requirements need to be considered in the numerical solution process [22]. Many efficient numerical techniques for solving fractional differential equations have been presented in the last decades such as the fractional finite volume method [23], neural network methods [24], Fourier spectral methods [25,26], radial basis functions [27], Adomian decomposition method [28], Haar wavelet method [29], operational matrix methods [30], and so forth. In the study on the anchor cable–rock and soil coupled creep model, the integer derivative method was widely used to solve this kind of problem in the field of geotechnical engineering [15,16,31,32]. The integer derivative method could accurately describe the coupled creep behavior of the anchor cable and the rock and soil mass and fully satisfy the accuracy requirements for practical engineering [31,33,34]. Therefore, the integer derivative method was used to establish the anchor cable–rock and soil coupled creep model of the pile–anchor structure in this paper.

The main structure of our study can be described in the following steps. We started by analyzing the instantaneous prestress loss caused by the deformation of the anchorage device and the waist beam. Then, we proposed a new anchor cable–rock and soil coupled creep model for pile–anchor structures, and verified the accuracy of the model through Chen's test. Additionally, we analyzed the prestress loss caused by the deformation of the anchorage device and the waist beam and proposed a calculation model to predict the prestress loss of anchor cables. Then, a prestress calculation model considering instantaneous prestress loss and long-term prestress loss was proposed. Finally, the accuracy and practicability of the anchor cable–rock and soil coupled creep model and the prestress loss calculation model were verified through an engineering example of Xingtai foundation excavation.

2. Factors of the Prestress Loss of Anchor Cables

The loss of the prestress has been throughout the entire life of the anchor cable work since the anchor cable was locked. There are many reasons for the loss of the prestress of the anchor cable, mainly including the following.

(1) The rebound deformation of the anchorage device [35–37]. The anchor clip is not stressed during the steel strand tension. When the jack is unloaded, the load acts on the clip, and the clip slips slightly with the shrinkage of the steel strand, resulting in prestress loss.

(2) The deflection deformation of the waist beam [38]. The prestress of anchor cables acts on the waist beam, which transfers the load to the anti-slide pile to stabilize the pile–anchor structure. Under the action of the prestress, the deflection deformation of the waist beam is generally calculated by the simply supported beam model.

(3) The creep deformation of the rock and soil mass [39–45]. As a composite of elastic, viscous, and plastics, the rock and soil mass has extremely complex mechanical properties and exhibits creep characteristics under deviatoric stress. The creep properties of the rock and soil mass with different mechanical properties are different.

(4) The creep deformation of the anchor cable [46]. The anchor cable is mainly composed of two parts: a free segment and an anchorage segment. The creep characteristic of

the free segment of the anchor cable is an instantaneous creep, and its deformation can be restored. The creep characteristic of the anchorage segment of the anchor cable is similar to that of the rock and soil mass.

It can be seen that the anchor cable–rock and soil coupled creep model of the pile-anchor structure must consider not only the mechanical properties of the rock and soil mass, but also the mechanical properties of the free segment and anchorage segment of the anchor cable [47–50]. In the calculation of the prestress loss of anchor cables, in addition to the long-term creep deformation, the prestress loss caused by the deformations of the anchorage device and the waist beam cannot be ignored.

3. Instantaneous Prestress Loss of Anchor Cable

In the pile–anchor structure, the prestress of the anchor cable often causes great deformations of the anchorage device and the waist beam. The instantaneous prestress loss caused by the deformations cannot be ignored, and the deformations are shown in Figure 1.

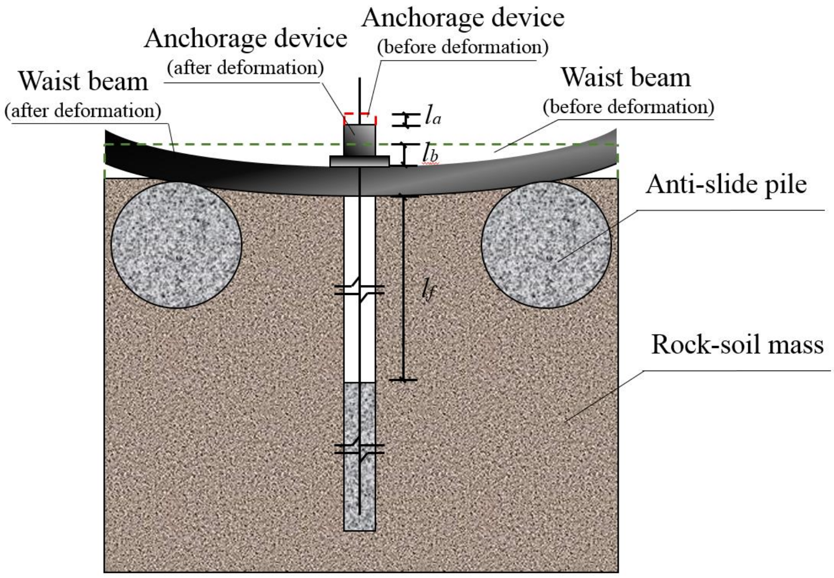

Figure 1. Schematic diagram of the deformations of anchorage device and waist beam.

3.1. The Prestress Caused by the Anchorage Device

After the anchor cable is tensioned and locked, the anchorage device will deform elastically and the clip will slip under the axial force. This process is bound to cause the prestress loss, and the equation for calculating the prestress loss of the anchor cable is as follows:

$$F_{\mathrm{a}} = A_{\mathrm{s}}\sigma_{\mathrm{a}} \tag{1}$$

$$\sigma_{\mathrm{a}} = \frac{l_{\mathrm{a}}}{l_{\mathrm{f}}}E_{\mathrm{a}} \tag{2}$$

3.2. The Prestress Loss Caused by the Waist Beam

The waist beam is the force transmission member between the anchor cable and the anti-slide pile. The deflection deformation of the waist beam under the anchor cable axial force causes the prestress loss. To calculate the waist beam deflection, it is generally required to adopt the mechanical model of the simply supported beam subjected to concentrated load in the middle of the span (Figure 1). The prestress loss caused by the waist beam deformation can be obtained as follows:

$$F_{\mathrm{b}} = A_{\mathrm{s}}\sigma_{\mathrm{b}} \tag{3}$$

$$\sigma_{\mathrm{b}} = \frac{l_{\mathrm{b}}}{l_{\mathrm{f}}} E_{\mathrm{a}} \tag{4}$$

$$l_{\mathrm{b}} = \frac{F{l_{\mathrm{p}}}^3}{48 E_{\mathrm{b}} I_{\mathrm{b}}} \tag{5}$$

4. The Anchor Cable–Rock and Soil Coupled Creep Model for the Pile–Anchor Structure

4.1. Anchor Cable–Rock and Soil Coupled Creep Model

The rock and soil mass creep model and the anchor cable creep model are composed of several elastoviscoplastic elements. The deformation of the rock and soil mass presents obvious characteristics of elasticity (instantaneous creep stage), viscoelasticity (decay creep stage), and viscoplasticity (steady creep stage). Anchor cables exhibit elastic (instantaneous creep stage) and viscoelastic (decay creep stage) deformation characteristics. The constitutive relationship of the anchor cable–rock and soil coupled creep model is composed of series and parallel connections of different mechanical elements.

At present, the coupled creep models of the anchor cable and the rock and soil mass include the following [31,32].

4.1.1. General Kelvin and Spring Element Parallel Coupled Creep Model

The model (Figure 2) reflects the instantaneous creep and decay creep state of the rock and soil mass, but the anchor cable creep model is simplified as a spring element, which cannot specifically reflect the creep characteristics of the free segment and the anchorage segment section of the anchor cable. According to the mechanical characteristics of the coupled creep model, its constitutive equation can be written as:

$$\sigma + \frac{\eta_{\mathrm{k}}}{E_{\mathrm{k}} + E_{\mathrm{h}}}\dot{\sigma} = \frac{E_{\mathrm{k}}E_{\mathrm{h}} + E_{\mathrm{h}}E_{\mathrm{s}} + E_{\mathrm{k}}E_{\mathrm{s}}}{E_{\mathrm{k}} + E_{\mathrm{h}}}\varepsilon + \frac{\eta_{\mathrm{k}}(E_{\mathrm{h}} + E_{\mathrm{s}})}{E_{\mathrm{k}} + E_{\mathrm{h}}}\dot{\varepsilon} \tag{6}$$

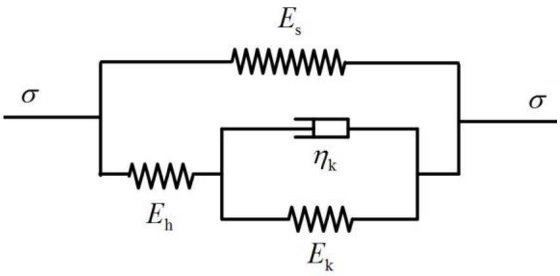

Figure 2. General Kelvin and spring element parallel coupled creep model.

4.1.2. General Kelvin and Maxwell Parallel Coupled Creep Model

Based on the general Kelvin and spring element parallel coupled creep model, an optimized coupled creep model (Figure 3) was proposed. The model fully considers the viscosity property of the anchor cable, and can describe the anchor cable–rock and soil coupled creep process more realistically. However, it defaults to a direct transition from instantaneous creep to steady state creep, and it ignores the decay creep stage of anchor cables, which is inconsistent with the actual creep of anchor cables. According to the stress–strain combination principle of the coupled creep model, the constitutive relationship is determined as:

$$\begin{gathered}\sigma + \frac{\eta_{\mathrm{k}}E_{\mathrm{m}}+\eta_{\mathrm{m}}E_{\mathrm{h}}+\eta_{\mathrm{m}}E_{\mathrm{k}}}{E_{\mathrm{m}}(E_{\mathrm{k}}+E_{\mathrm{h}})}\dot{\sigma} + \frac{\eta_{\mathrm{m}}\eta_{\mathrm{k}}}{E_{\mathrm{m}}(E_{\mathrm{k}}+E_{\mathrm{h}})}\ddot{\sigma} = \frac{E_{\mathrm{h}}E_{\mathrm{k}}}{E_{\mathrm{k}}+E_{\mathrm{h}}}\varepsilon + \\ \frac{\eta_{\mathrm{k}}E_{\mathrm{h}}E_{\mathrm{m}}+\eta_{\mathrm{m}}E_{\mathrm{h}}E_{\mathrm{k}}+\eta_{\mathrm{m}}E_{\mathrm{h}}E_{\mathrm{m}}+\eta_{\mathrm{m}}E_{\mathrm{m}}E_{\mathrm{k}}}{E_{\mathrm{m}}(E_{\mathrm{k}}+E_{\mathrm{h}})}\dot{\varepsilon} + \frac{\eta_{\mathrm{k}}\eta_{\mathrm{m}}(E_{\mathrm{k}}+E_{\mathrm{h}})}{E_{\mathrm{m}}(E_{\mathrm{k}}+E_{\mathrm{h}})}\ddot{\varepsilon}\end{gathered} \tag{7}$$

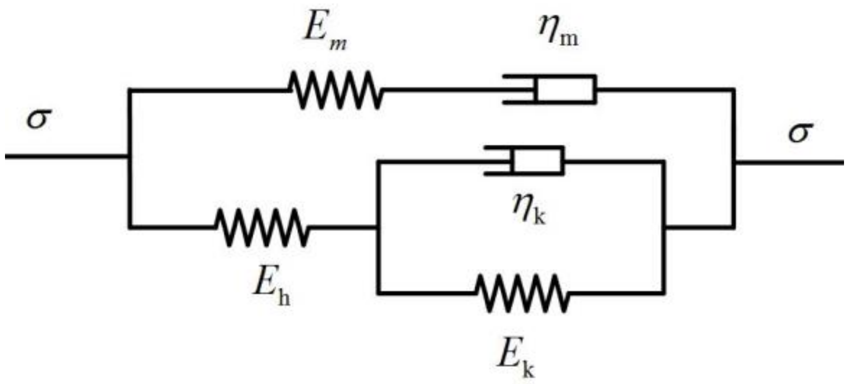

Figure 3. General Kelvin and Maxwell parallel coupled creep model.

4.2. The Anchor Cable–Rock and Soil Coupled Creep Model of the Pile–Anchor Structure

The coupled creep model of the anchor cable and the rock and soil mass of the pile–anchor structure is different from that of the traditional roadway support. In roadway support, the prestress of anchor cables is applied to the surface of the rock and soil mass through the plate. In this process, the sum of deformations of the free segment and the anchorage segment of the anchor cable is equal to the deformation of the rock and soil mass. The anchor cable creep model and the rock and soil creep model are parallel relationships. In the pile–anchor structure (Figure 4), the anti-slide pile makes the anchor cable prestress directly act on the rigid pile instead of the rock and soil mass through the waist beam. At this time, the anchorage segment of the anchor cable and the rock and soil mass contact and interact with each other, and the deformations are coordinated. The stress of the free segment is equal to the coupled stress between the anchorage segment and the rock and soil mass. In the coupled creep model of the pile–anchor structure, the creep model of the anchorage segment and the creep model of the rock and soil mass are parallel relationships, and they are connected in series with the creep model of the free segment. Since the rigidity of the anchorage segment of the anchor cable is much greater than that of the rock and soil mass, when the rock and soil mass is in the instantaneous creep stage, the anchorage segment can be regarded as a rigid body and does not enter the instantaneous creep stage. Therefore, the coupled creep model of the anchor cable and the rock and soil mass of the pile–anchor structure is proposed as shown in Figure 5.

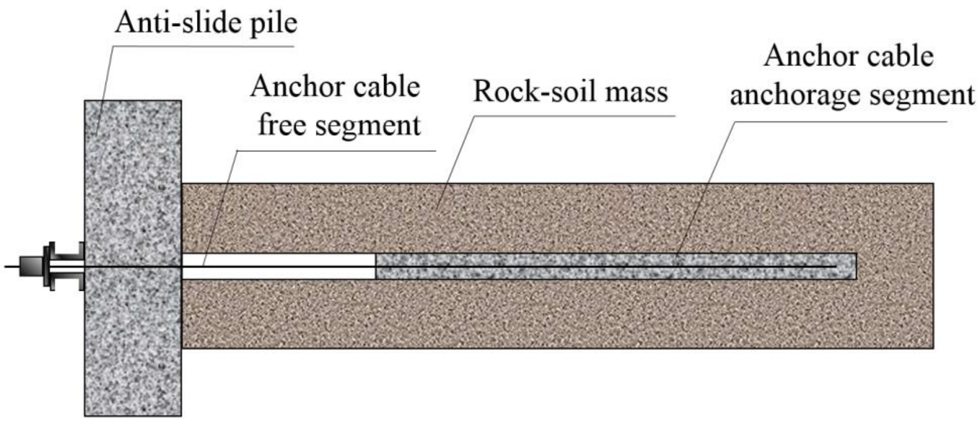

Figure 4. Schematic diagram of pile–anchor structure.

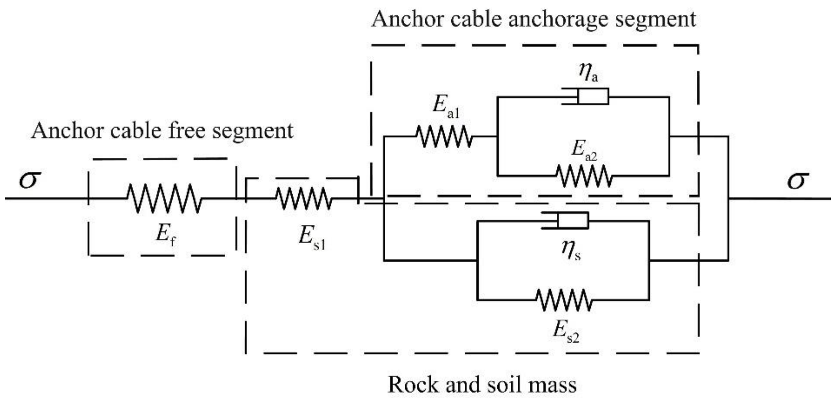

Figure 5. The anchor cable–rock and soil coupled creep model.

According to the coupled creep model of the anchor cable and the rock and soil mass of the pile–anchor structure, the constitutive equation is deduced as:

$$A\ddot{\sigma} + B\dot{\sigma} + \sigma = C\ddot{\varepsilon} + D\dot{\varepsilon} + E\varepsilon \tag{8}$$

where

$$A = \frac{\eta_{\mathrm{s}}\eta_{\mathrm{a}}(E_{\mathrm{s1}} + E_{\mathrm{f}})}{E_{\mathrm{a1}}[E_{\mathrm{f}}(E_{\mathrm{a2}}E_{\mathrm{s1}}E_{\mathrm{s2}}) + E_{\mathrm{s1}}(E_{\mathrm{a2}} + E_{\mathrm{s2}})] + E_{\mathrm{a2}}[E_{\mathrm{s1}}(E_{\mathrm{f}} + E_{\mathrm{s2}}) + E_{\mathrm{a2}}E_{\mathrm{s2}}]}$$

$$B = \frac{\eta_{\mathrm{a}}[E_{\mathrm{s1}}(E_{\mathrm{a1}} + E_{\mathrm{s2}}) + E_{\mathrm{f}}(E_{\mathrm{a1}} + E_{\mathrm{s1}} + E_{\mathrm{s2}})] + \eta_{\mathrm{s}}(E_{\mathrm{a1}} + E_{\mathrm{a2}})(E_{\mathrm{f}} + E_{\mathrm{s1}})}{E_{\mathrm{a1}}[E_{\mathrm{f}}(E_{\mathrm{a2}}E_{\mathrm{s1}}E_{\mathrm{s2}}) + E_{\mathrm{s1}}(E_{\mathrm{a2}} + E_{\mathrm{s2}})] + E_{\mathrm{a2}}[E_{\mathrm{s1}}(E_{\mathrm{f}} + E_{\mathrm{s2}}) + E_{\mathrm{a2}}E_{\mathrm{s2}}]}$$

$$C = \frac{\eta_{\mathrm{s}}\eta_{\mathrm{a}}E_{\mathrm{s1}}E_{\mathrm{f}}}{E_{\mathrm{a1}}[E_{\mathrm{f}}(E_{\mathrm{a2}}E_{\mathrm{s1}}E_{\mathrm{s2}}) + E_{\mathrm{s1}}(E_{\mathrm{a2}} + E_{\mathrm{s2}})] + E_{\mathrm{a2}}[E_{\mathrm{s1}}(E_{\mathrm{f}} + E_{\mathrm{s2}}) + E_{\mathrm{a2}}E_{\mathrm{s2}}]}$$

$$D = \frac{E_{\mathrm{s1}}E_{\mathrm{f}}[\eta_{\mathrm{a}}(E_{\mathrm{a1}} + E_{\mathrm{s1}}) + \eta_{\mathrm{s}}(E_{\mathrm{a1}} + E_{\mathrm{a2}})]}{E_{\mathrm{a1}}[E_{\mathrm{f}}(E_{\mathrm{a2}}E_{\mathrm{s1}}E_{\mathrm{s2}}) + E_{\mathrm{s1}}(E_{\mathrm{a2}} + E_{\mathrm{s2}})] + E_{\mathrm{a2}}[E_{\mathrm{s1}}(E_{\mathrm{f}} + E_{\mathrm{s2}}) + E_{\mathrm{a2}}E_{\mathrm{s2}}]}$$

$$E = \frac{E_{\mathrm{s1}}E_{\mathrm{f}}[E_{\mathrm{a1}}E_{\mathrm{a2}} + E_{\mathrm{a2}}E_{\mathrm{s2}} + E_{\mathrm{a1}}E_{\mathrm{s1}}]}{E_{\mathrm{a1}}[E_{\mathrm{f}}(E_{\mathrm{a2}}E_{\mathrm{s1}}E_{\mathrm{s2}}) + E_{\mathrm{s1}}(E_{\mathrm{a2}} + E_{\mathrm{s2}})] + E_{\mathrm{a2}}[E_{\mathrm{s1}}(E_{\mathrm{f}} + E_{\mathrm{s2}}) + E_{\mathrm{a2}}E_{\mathrm{s2}}]}$$

4.2.1. Creep Equation of the Coupled Creep Model

A constant load is applied to the anchor cable where, $\sigma = \sigma_{\mathrm{c}} = \sigma_{\mathrm{const}}$. According to Equation (8), the following creep equation is obtained:

$$\sigma_{\mathrm{c}} = C\ddot{\varepsilon} + D\dot{\varepsilon} + E\varepsilon \tag{9}$$

The creep equation is a quadratic non-homogeneous differential equation of one variable. According to the differential equation solving rule, the following can be obtained:

$$\varepsilon_{\mathrm{c}}(t) = C_1 e^{(r_1 t)} + C_2 e^{(r_2 t)} + \frac{\sigma_c}{E} \tag{10}$$

The initial condition of differential equations: When a constant load is applied instantaneously, the free segment of the anchor cable and the rock and soil mass will only produce instantaneous creep, namely, $\varepsilon_{\mathrm{t=0}} = \sigma_{\mathrm{c}}/H$, there, $H = E_{\mathrm{s1}}E_{\mathrm{f}}/(E_{\mathrm{f}} + E_{\mathrm{s1}})$. The assumption: Under a constant load, there must be a certain moment at which the strain tends to stabilize and no longer increases with time. At this time, the strain derivative is 0, namely, $\dot{\varepsilon}_{t=t_s} = 0$. The initial condition and the assumption are substituted into differential Equation (10), and C_1 and C_2 are deduced as:

$$C_1 = \frac{\sigma_{\mathrm{c}} r_2 (H - E) e^{r_2 t_{\mathrm{s}}}}{EH(r_1 e^{r_1 t_{\mathrm{s}}} - r_2 e^{r_2 t_{\mathrm{s}}})} \tag{11}$$

$$C_2 = \frac{\sigma_c r_1 (E-H) e^{r_1 t_s}}{EH(r_1 e^{r_1 t_s} - r_2 e^{r_2 t_s})} \tag{12}$$

4.2.2. Relaxation Equation of the Coupled Creep Model

When the anchor cable is locked, the strain of the coupled creep system is constant and the stress gradually relaxes. Defining $\varepsilon = \varepsilon_c = \varepsilon_{const}$, the constitutive Equation (8) can be expressed as:

$$A\ddot{\sigma} + B\dot{\sigma} + \sigma = E\varepsilon_c \tag{13}$$

Solving the differential Equation (13), the following can be obtained:

$$\sigma(t) = C_3 e^{r_3 t} + C_4 e^{r_4 t} + E\varepsilon_c \tag{14}$$

The initial condition of differential equations: At the moment when the initial strain is applied, the elastic deformation of the free segment of the anchor cable and the rock and soil mass is completed instantly, and the strain is ε_c, namely, $\sigma_{t=0} = H\varepsilon_c$. The assumption: In the stress relaxation stage of the coupled creep model, there must be a certain moment at which the stress no longer decreases and remains constant. At this time, the stress derivative is 0, that is, $\dot{\sigma}_{t=t_v} = 0$.

According to the initial condition and assumption, C_3 and C_4 can be expressed as:

$$C_3 = \frac{\varepsilon_c r_4 (E-H) e^{r_4 t_v}}{r_3 e^{r_3 t_v} - r_4 e^{r_4 t_v}} \tag{15}$$

$$C_4 = \frac{\varepsilon_c r_4 (E-H) e^{r_4 t_v}}{r_3 e^{r_3 t_v} - r_4 e^{r_4 t_v}} \tag{16}$$

In the pile–anchor structure, the anchor cable should meet the following assumptions:

1. The total axial force of the steel strands in the free segment is equal to the locked prestress;
2. The total axial force of the anchor cable is evenly distributed to each steel strand;
3. No loss of the prestress during the transmission of the free segment of the anchor cable; and
4. The group anchor effect does not occur in the support system.

The prestress of the anchor cable can be expressed as:

$$C_4 = \frac{\varepsilon_c r_4 (E-H) e^{r_4 t_v}}{r_3 e^{r_3 t_v} - r_4 e^{r_4 t_v}} \tag{17}$$

4.3. Model Test Verification

To verify the feasibility of the coupled creep model, we used Chen's classic soft rock model test [51] to test the prediction ability of the creep equation and the relaxation equation. The model box and anchor rod size parameters used in the test are shown in Figure 6. The simulated material of the anchor rod was a copper tube with a size of φ6 × 2 mm and an elastic modulus of 1.32×10^5 Mpa. The cement grade of anchor rod grouting material was #425, and the weight ratio of cement, water, and accelerator was 1 to 0.64 to 0.2. The model medium material was yellow clay sand, and its physical and mechanical parameters are shown in Table 1.

Table 1. Physical and mechanical parameters of yellow clay sand.

Soil Layer	Moisture Content/%	Density /(kN/m^3)	Uniaxial Compressive Strength/MPa	Uniaxial Tensile Strength /MPa	Elastic Modulus /MPa	Cohesion /kPa	Internal Friction Angle/(°)
Yellow clay sand	16.5	20	0.15	0.04	20.66	11	19

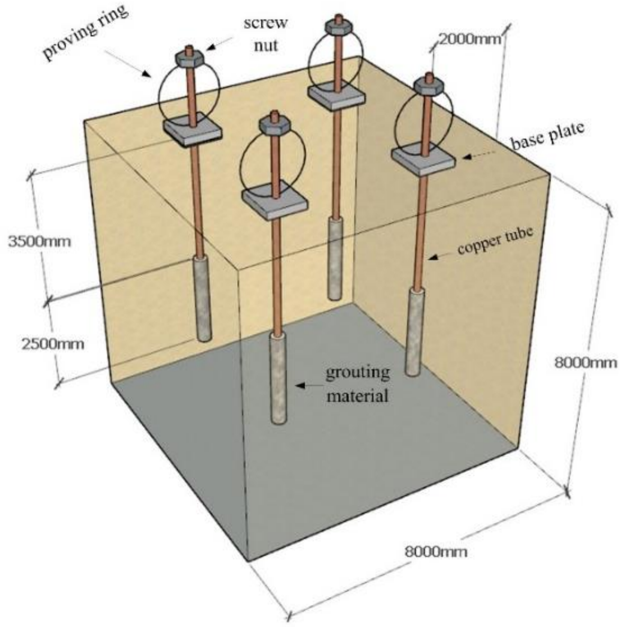

Figure 6. Soft rock test model.

Figure 7 is the comparison diagram of the data curves of the #2–#4 anchor rods' creep test and the model prediction curves, in which the #1 anchor rod failed to extract the monitoring data of the whole test due to equipment failure. As shown in Table 2, the #2–#4 anchor rod test data were highly close to the model calculation data, and the correlation coefficients of prediction results were 0.9954, 0.9962, and 0.9989, respectively. The model showed an excellent prediction effect. During the test, the constant pressure load directly acts on the top of the copper pipe, and the copper pipe transmits the pressure to the grouting section. The interaction between the grouting section and the yellow clay sand forms a coupled creep system. The principle is the same as that of the coupled creep model in the pile–anchor structure, so the prediction results of the model are highly consistent with the test data.

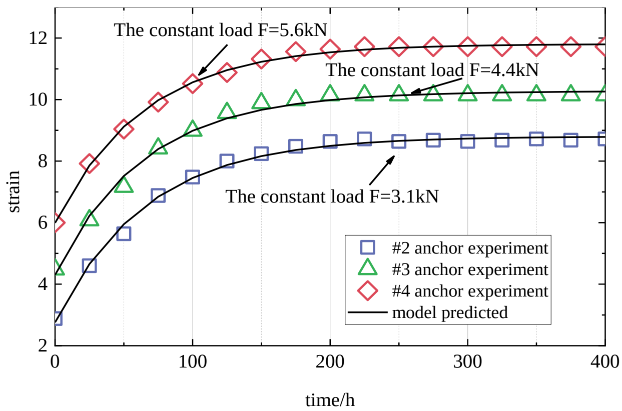

Figure 7. The #2–#4 anchor rods' creep test and prediction curves.

Table 2. Correlation coefficient between model test and prediction.

Types of Tests	Anchor Rods: Creep Test			Anchor Rods: Relaxation Test			
Anchor rod numbers	#2	#3	#4	#1	#2	#3	#4
Correlation coefficients	0.9954	0.9962	0.9989	0.9744	0.9847	0.9710	0.9709

The data curves of the prestress relaxation test of the #1–#4 anchor rods and model prediction curves are shown in Figure 8. Regardless of the test curves or the prediction curves, the decay law of the anchor rod axial force with time was consistent, and the prediction results were close to the test data. As shown in Table 2, the correlation coefficients of the prediction results of #1–#4 anchor rods were 0.9744, 0.9847, 0.9710, and 0.9709, respectively, and the prestress relaxation prediction effect was good. Comparing Figure 7 with Figure 8, it was not difficult to find that the accuracy of the prestress relaxation prediction curves was lower than that of the creep prediction curves. The reason is that the coupled creep system of the test was similar to the coupled creep system of the pile–anchor structure, and the coupled creep model was completely applicable. In the anchor rod prestress relaxation test, the prestress acts on the soil medium through the plate, which was slightly different from the mechanical behavior of the coupled creep model, so the prediction accuracy decreased.

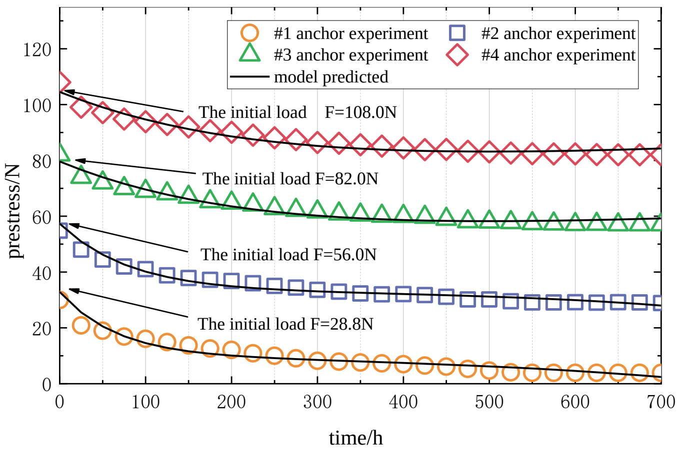

Figure 8. The #1–#4anchor rods' relaxation test and prediction curves.

5. The Anchor Cable Prestress Loss Calculation Model for the Pile–Anchor Structure

After the anchor cable is locked, it will inevitably produce prestress loss due to the rebound deformation of the anchorage device, the deflection deformation of the waist beam, and the coupled creep of the anchor cable and the rock and soil mass. Meanwhile, the prestress loss equation is a function of time. The prestress loss calculation model can be expressed as follows:

$$T(t) = F_{\mathrm{a}} + F_{\mathrm{b}} + F_{\mathrm{c}}(0) - F_{\mathrm{c}}(t) \tag{18}$$

The calculation model of the prestress loss can be obtained by substituting Equations (1)–(5) and Equations (14)–(17) into Equation (18) as follows:

$$T(t) = \frac{A_{\mathrm{s}} l_{\mathrm{a}} E_{\mathrm{s}}}{l_{\mathrm{f}}} + \frac{A_{\mathrm{s}} {l_{\mathrm{p}}}^3 E_{\mathrm{s}} F}{48 E_{\mathrm{b}} I_{\mathrm{b}} l_{\mathrm{f}}} + A_{\mathrm{s}}\left[\left(C_3\left(1 - e^{r_3 t}\right) + C_4\left(1 - e^{r_4 t}\right)\right)\right] \tag{19}$$

The ratio of prestress loss value and initial prestress value is denoted as the prestress loss ratio, which is used to indicate the degree of prestress loss of the anchor cable. The prestress loss ratio can be obtained as follows:

$$\omega(t) = \frac{T(t)}{F} \tag{20}$$

6. Calculation and Analysis of Engineering Cases

6.1. Project Overview

The foundation pit was located in Xingtai City, Hebei Province. According to the results of drilling identification, geotechnical test, and in situ test, the soil layer can be divided into five geological exploration layers from bottom to top, which are miscellaneous fill, silt①, silt②, clay①, and clay②. During the field survey, it was discovered that the groundwater level was about 2.5 m deep, and the groundwater was pore phreatic water. Soil samples were tested in the laboratory, and the physical and mechanical parameters of the soil layers are shown in Table 3.

Table 3. Physical and mechanical parameters of soil layers.

Layer Number	Soil Layer	Thickness/m	Density /(kN/m^3)	Buoyancy Density/(kN/md)	Cohesion /kPa	Internal Friction Angle/(°)	Ultimate Bond Strength/kPa
1	Miscellaneous fill	1.70	15.0	—	3.00	8.00	28
2	Silt①	4.20	19.0	9.0	15.30	22.60	64
3	Silt②	5.20	19.2	9.2	14.50	25.30	65
4	clay①	8.00	19.1	9.1	22.30	11.40	60
5	clay②	10.00	19.3	9.3	—	—	61

The foundation pit had a length of 94.6 m from north to south and a width of 84.4 m from east to west. The maximum excavation depth of the foundation pit was 10.5 m. As shown in Figure 9, the support structure for the foundation pit was anti-slide piles, top beams, waist beams, and prestressed anchor cables. The cross-section size of the top beam was 1000 mm × 800 mm. The anti-slide pile was 1200 mm in diameter and was poured with C30 reinforced concrete. The longitudinal reinforcement was HRB400, and the spiral stirrup was HPB300. The waist beam was welded by two 20a channel steels in parallel. The geometric and material parameters of the anchor cables are shown in Table 4.

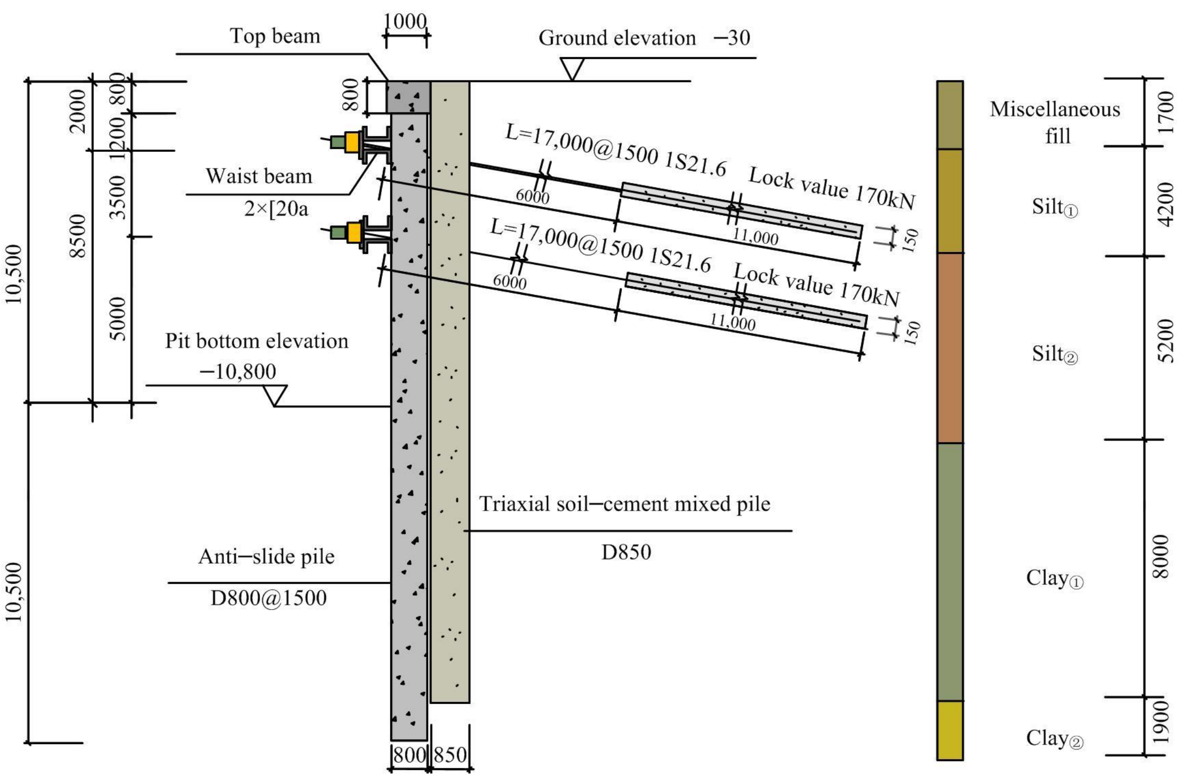

Figure 9. Schematic diagram of the pile–anchor support.

Table 4. The geometric and material parameters of the anchor cables.

Serial Number	Position	Elevation/m	Total Length/m	Length of Anchorage Section/m	Diameter of Hole/mm	Mortar Grade	Grade of Reinforcement	Standard	Locked Value/kN
1	North side middle	−2.0	22.0	13.0	150	C20	HRB400	1s21.6	210
2	North side middle	−5.5	20.0	12.0	150	C20	HRB400	1s21.6	200
3	West side middle	−2.0	18.0	11.0	150	C20	HRB400	1s21.6	180
4	West side middle	−5.5	17.0	11.0	150	C20	HRB400	1s21.6	170
5	East side middle	−2.0	18.0	11.0	150	C20	HRB400	1s21.6	180
6	East side middle	−5.5	17.0	11.0	150	C20	HRB400	1s21.6	170
7	South side middle	−2.0	16.0	10.0	150	C20	HRB400	1s21.6	120
8	South side middle	−5.5	15.0	10.0	150	C20	HRB400	1s21.6	110

To study the prestress loss of anchor cables, eight anchor cables in the middle of the foundation pit were randomly selected. Before the anchor cables were tensioned, an axial force sensor was installed under the anchorage device of each anchor cable. The sensors used for monitoring prestress were HF-201 vibrating wire heart-piercing sensors, and the 609 vibrating wire reader was used to collect the prestress data of the anchor cables. The prestress data were collected and recorded manually at 9:00 am every morning. Because the tensioning times of the anchor cables at different positions were different, the initial monitoring times of the anchor cables were different. All anchor cables ended prestress monitoring on 30 July 2017.

6.2. Comparative Analysis of the Monitoring and Model Calculation Results

As shown in Figure 10, it can be seen from the anchor cable monitoring date that the prestress of the anchor cables experiences varying degrees of loss after the cables are locked. The #3 anchor cable had the lowest prestress loss, which was only 10 kN. Since the #1 anchor cable was applied with the largest prestress, its prestress loss was the most serious, and the prestress attenuated to the stable stage for the longest time. Although the #2–#8 anchor cables were tensioned at different times, the prestressing attenuation tended to be stable within 10 days after each anchor cable was tensioned. Due to the influence of objective factors such as precipitation, temperature, and dynamic and static load around the foundation pit, there will be a small range of fluctuations in the attenuation process of prestress.

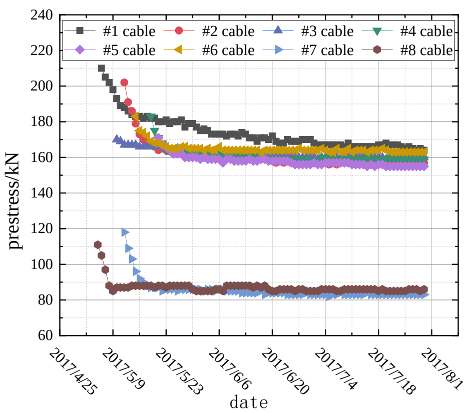

Figure 10. Prestress monitoring values of #1–#8 anchor cables.

The calculation model of the prestress loss of the anchor cable of the pile–anchor structure is mainly composed of two parts. One part is composed of instantaneous deformations such as the anchorage device rebound deformation and the waist beam deflection deformation. This part of the prestress loss is eliminated by measures such as overtension. Comparing the actually locked load with the model calculated locked load, the values of the two were similar. The results in Table 5 indicate that the maximum calculation error of the instantaneous prestress loss was 7.47%, and the minimum error was only 1.27%.

Table 5. Comparison of the monitoring and model calculation results for the prestress of the cables.

	Instantaneous Deformation				Creep Deformation				
Anchor Cable	**Implement Tension Load /kN**	**Actual Locked Load /kN**	**Calculate Locked Load /kN**	**Error**	**Initial Creep Actual Prestress/kN**	**Initial Creep Calculation Prestress/kN**	**Final Creep Actual Prestress/kN**	**Final Creep Calculation Prestress/kN**	**Correlation Coefficient**
#1	300	210	194.32	7.47%	210	215.03	164	164.32	0.9709
#2	295	202	188.51	6.68%	202	200.35	157	158.58	0.9654
#3	280	170	160.17	5.78%	170	171.72	155	154.56	0.9414
#4	285	183	169.83	7.19%	183	181.51	159	159.87	0.9481
#5	280	171	160.17	6.33%	171	171.90	160	159.88	0.9539
#6	285	183	169.83	7.19%	183	181.94	164	163.95	0.9672
#7	260	118	122.16	3.53%	118	118.16	83	83.91	0.9797
#8	250	111	112.41	1.27%	111	110.51	86	85.2	0.9781

The other part is the coupled creep of the anchor cable and the rock and soil mass under long-term load, and the prestress loss can be calculated by the coupled creep model. The curves in Figure 11 indicate that the minimum correlation coefficient of the prediction curves was 0.9414, and the maximum was 0.9781. The time for the prestress of the #1–#8 anchor cables to reach a stable stage was also approximately the same in the monitoring and model predicted curves. The coupled creep model could effectively describe the creep behavior of the anchor cable and the rock and soil mass. However, affected by precipitation, temperature, and dynamic and static loads on the surrounding roads, the monitoring curves appeared as transient fluctuations. The creep coupled model can well reveal the development law of the actual prestress of the anchor cable, but it cannot be used to predict the time and amplitude of the prestress fluctuation caused by external factors.

The comparative data between the actual loss ratio and the calculated loss ratio caused by deformations of the anchorage device and the waist beam are shown in Figure 12. The actual prestress loss ratios of the #1~#6 anchor cables were less than the calculated prestress loss ratios, and the model calculation tended to be conservative. The calculated value of the #7–#8 anchor cable prestress loss ratios were the same as the actual monitoring values. The reason is that when the anchor cables are tensioned and locked, the operation of workers is not standard, which causes the actual loss ratios of the #7–#8 anchor cables to increase. The instantaneous prestress loss ratios calculated by the model of the #1–#8 anchor cables were 35.2%, 36.1%, 42.8%, 40.4%, 42.8%, 40.4%, 53.0%, and 55.0%, respectively, which are consistent with the research conclusion of Tang [52]. Tang indicated that when the anchor cable was tensioned to locked, the maximum loss ratio of prestress caused by the anchor device and the waist beam was 53.4%, and the minimum loss ratio was 24.5%.

The relationship curve between creep loss ratio and time is shown in Figure 13. The prestress loss ratio increased rapidly first, and then remained basically unchanged over time. It shows that the creep effect will end at a certain moment, and after that, with the further delay of time, the prestress loss of the anchor cable disappears.

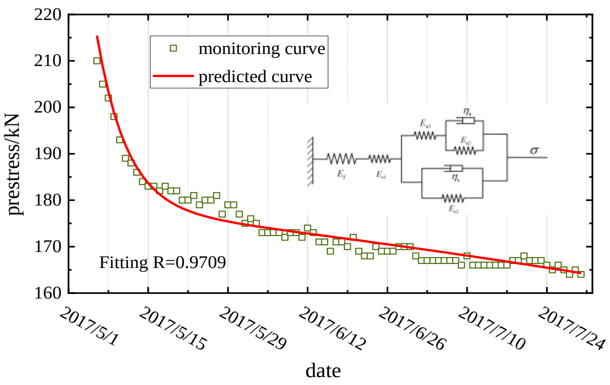

(**a**) #1 anchor cable

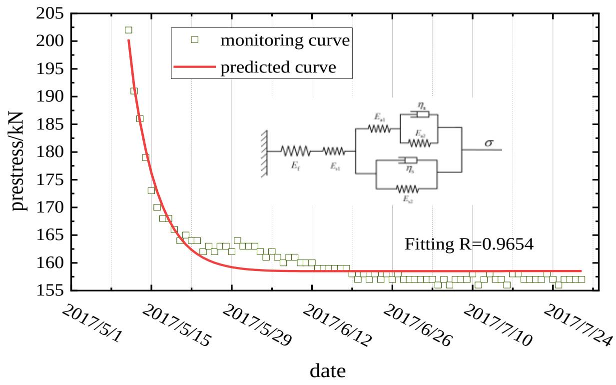

(**b**) #2 anchor cable

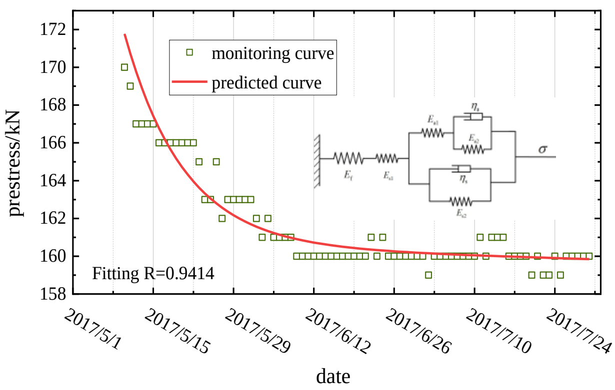

(**c**) #3 anchor cable

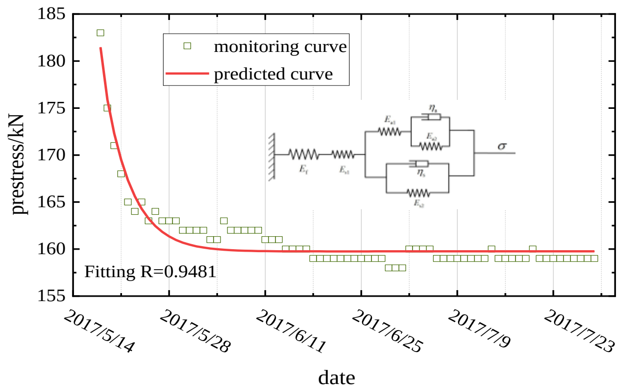

(**d**) #4 anchor cable

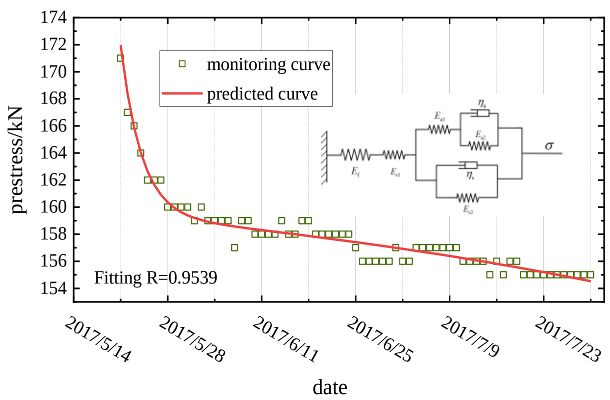

(**e**) #5 anchor cable

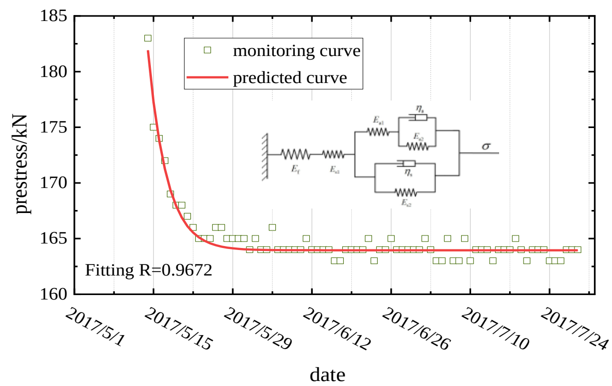

(**f**) #6 anchor cable

Figure 11. *Cont.*

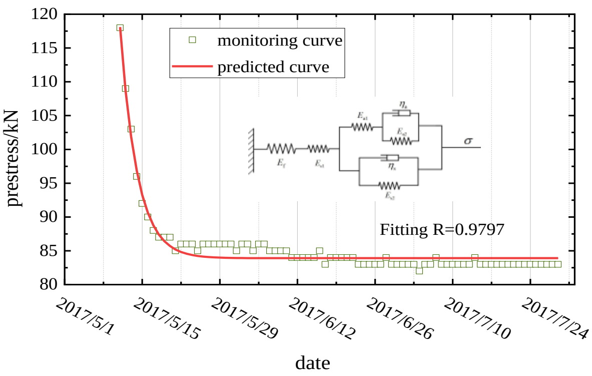

(**g**) #7 anchor cable

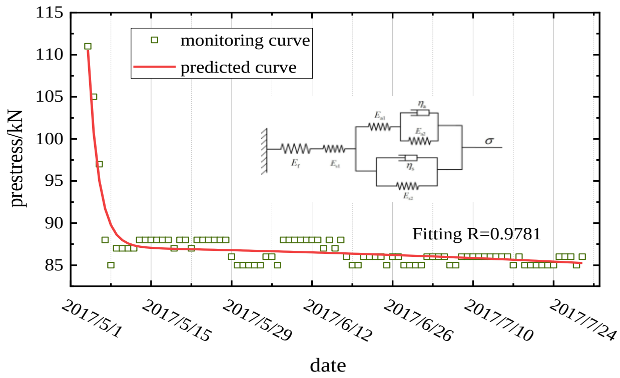

(**h**) #8 anchor cable

Figure 11. Comparison of monitoring and prediction prestress of the anchor cables.

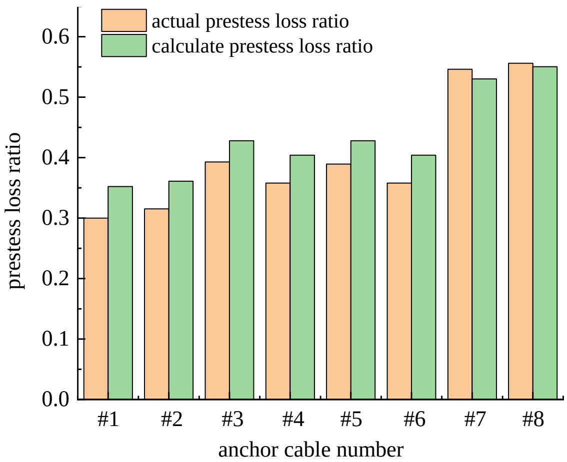

Figure 12. Comparison of actual and calculated prestress loss ratio of the anchor cable.

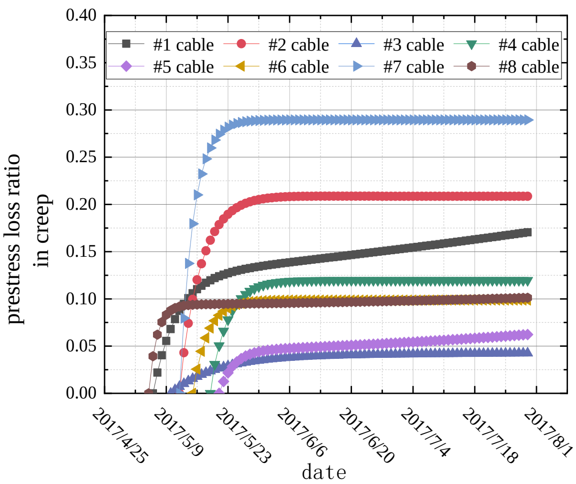

Figure 13. The curves of creep prestress loss ratio with time.

7. Discussion

The biggest challenge in the study of the prestress loss of anchor cable in the pile–anchor structure is to establish the coupled creep model of the anchor cable and rock and soil mass considering the action of anti-slide pile. In this paper, the interaction relationship between anti-sliding pile, anchor cable, and rock and soil mass was clarified, and the coupled creep characteristics of the anchor cable and rock and soil mass under the action of anti-sliding pile were defined. Based on this, a new coupled creep model was proposed, and a prestress loss calculation model of anchor cable in the pile–anchor structure was established. The calculation results are consistent with the monitoring data, and the model has important engineering application value. However, whether it is the instantaneous prestress loss caused by the anchorage device and the waist beam or the long-term prestress loss caused by the anchor cable–rock and soil coupled creep, the calculation results of the model had certain errors. The error of the instantaneous prestress loss calculation model has the following two aspects. (1) When calculating the deflection of the waist beam in the instantaneous prestress loss model, it is assumed that the mid-span load of the waist beam is the implementation tension load. However, in actual engineering, due to the rebound deformation of the anchorage device and the deflection deformation of the waist beam, the mid-span tensile load continues to decrease, so the actual deflection of the waist beam is less than the calculated deflection. The calculation of the instantaneous loss of prestress tends to be conservative. (2) The deflection calculation model of the waist beam is simplified to a simply supported beam model. The actual mechanical model of the waist beam is similar to the continuous beam model. Therefore, the calculated deformation of the waist beam is greater than the actual deformation, which causes the calculated prestress loss to be large.

In this paper, the integer derivative method was used to establish the coupled creep model. However, the fractional derivative method was applied to creep research in other fields and achieved some results. Therefore, the fractional derivative method can be used as a new method for the coupled creep study of anchor cable and rock and soil mass in the follow-up research. In addition, the coupled creep model was established based on certain assumptions. For example, the anti-slide pile is completely rigid, and the rock and soil mass is homogeneous and isotropic, which is not the case in actual engineering.

8. Conclusions

In light of the interaction between the waist beam, the anti-slide pile, the anchor cable, and the rock and soil mass, the anchor cable prestress loss calculation model of the pile–anchor structure was established, and its accuracy was verified by engineering cases. In the calculation model, the instantaneous prestress loss caused by the deformations of the waist beam and the anchor cable was considered, and the long-term prestress loss caused by the coupled creep of the anchor cable and the rock and soil mass was considered.

According to the characteristics of the pile–anchor structure, a new coupled creep model of the anchor cable and the rock and soil mass was proposed, and the creep equation and relaxation equation of the model were deduced. The new coupled creep model is not only suitable for predicting the prestress loss value of the anchor cable, but can also be used to predict the time required for the prestress value to reach the stable stage. However, the coupled creep model cannot be used to describe the time and amplitude of the weak fluctuation of the long-term prestress of anchor cables caused by precipitation, temperature, and surrounding dynamic and static loads.

Comparing the prestress loss model calculation results with the monitoring data, it was found that the maximum calculation error of the instantaneous prestress loss was 7.47%, and the minimum correlation coefficient of the long-term prestress loss was 0.9481. Although there are certain errors in the model calculation results, it could fully meet the engineering needs and conform to the actual situation, and the prestress loss calculation model has significant engineering application value.

Author Contributions: Conceptualization, X.G., J.J. and G.M.; Methodology, X.G., J.J., G.M. and X.B.; Software, X.G. and L.Z.; Validation, X.G., J.J. and X.L.; Data curation, L.Z. and X.L.; Writing—original draft preparation, X.G. and J.J.; Writing—review and editing, G.M. and X.B; Visualization, X.G.; Supervision, J.J. and G.M. All authors have read and agreed to the published version of the manuscript.

Funding: This research was funded by the National Key Research and Development Program of China, grant number 2018YFC1505302 and the National Natural Science Foundation of China, Grant No. 51678112.

Institutional Review Board Statement: Not applicable.

Informed Consent Statement: Not applicable.

Data Availability Statement: The data presented in this study are available on request from the corresponding author. The data are not publicly available as there are no data uploaded on the website.

Conflicts of Interest: The authors declare no conflict of interest. The funders had no role in the design of the study; in the collection, analyses, or interpretation of data; in the writing of the manuscript, or in the decision to publish the results.

Notation

σ_a	Axial stress loss due to deformation of anchorage device
σ_b	Axial stress loss due to deformation of waist beam
σ_s	Axial stress of free segment of anchor cable
F	Prestress of anchor cable
A_s	Equivalent cross-sectional area of free segment of anchor cable
l_a	Sum of rebound value of anchorage device and slip value of clip
l_f	Length of free segment of anchor cable
l_b	Deflection deformation of waist beam
l_p	Distance between adjacent piles
I_b	Moment of inertia of waist beam
E_a	Elastic modulus of anchor cable
E_b	Elastic modulus of waist beam
E_s	Young's moduli of spring element of anchor cable in Figure 2
E_h	Young's moduli of spring element of rock and soil mass in Figures 2 and 3
E_k	Young's moduli of another spring element of rock and soil mass in Figures 2 and 3
η_k	Coefficient of viscosity of dashpot element of rock and soil mass in Figures 2 and 3
E_m	Young's moduli of spring element of anchor cable in Figure 3
η_m	coefficient of viscosity of dashpot element of anchor cable in Figure 3
E_f	Young's moduli of spring element of free segment of anchor cable in Figure 5
E_{a1}	Young's moduli of spring element of anchorage segment of anchor cable in Figure 5
E_{a2}	Young's moduli of another spring element of anchorage segment of anchor cable in Figure 5
E_{s1}	Young's moduli of spring element of rock and soil mass in Figure 5
E_{s2}	Young's moduli of another spring element of rock and soil mass in Figure 5
η_a	Coefficient of viscosity of the dashpot element of anchorage segment of anchor cable in Figure 5
η_s	Coefficient of viscosity of the dashpot element of rock and soil mass in Figure 5

References

1. Huang, Y.; Xu, X.; Liu, J.J.; Mao, W.W. Centrifuge Modeling of Seismic Response and Failure Mode of a Slope Reinforced by a Pile-Anchor Structure. *Soil Dyn. Earthq. Eng.* **2020**, *131*, 106037. [CrossRef]
2. Li, X.C.; Xu, R.; Yang, W.; Li, P.G.; Yang, K.; Zhang, W.Y. Experimental Study on Distribution of Landslide Thrust in Pile-Anchor Structure Based on Photoelastic Technique. *Materials* **2020**, *13*, 1358. [CrossRef] [PubMed]
3. Peng, J.S.; Liu, H.X.; Zhao, Y.B.; Liang, K. Failure Mode and Pullout Capacity of Anchor Piles in Soils with Cohesive and Cohesionless Properties. *Mar. Georesour. Geotechnol.* **2020**, *38*, 1056–1069. [CrossRef]
4. Sun, J.K.; Wang, S.P.; Shi, X.J.; Wu, F.; Zeng, L.Y. Study on the Design Method for the Deformation State Control of Pile-Anchor Structures in Deep Foundation Pits. *Adv. Civ. Eng.* **2019**, *2019*, 9641674. [CrossRef]
5. Li, Y.X.; Zhang, W.Y.; Jiang, N.S.; Li, H. Surface Settlement Damage Model of Pile-Anchor Supporting Structure in Deep Excavation. *Adv. Civ. Eng.* **2020**, *2020*, 1907526. [CrossRef]
6. El Menoufy, A.; Soudki, K. Effects of Various Environmental Exposures and Sustained Load Levels on the Service Life of Postinstalled Adhesive Anchors. *J. Mater. Civ. Eng.* **2014**, *26*, 863–871. [CrossRef]
7. Benmokrane, B.; Ballivy, G. Five-Year Monitoring of Load Losses on Prestressed Cement-Grouted Rock Anchors. *Can. Geotech. J.* **1991**, *28*, 668–677. [CrossRef]
8. Zhang, G.B.; Chen, C.F.; Zornberg, J.G.; Morsy, A.M.; Mao, F.S. Interface Creep Behavior of Grouted Anchors in Clayey Soils: Effect of Soil Moisture Condition. *Acta Geotech.* **2020**, *15*, 2159–2177. [CrossRef]

9. Yang, M.J.; Zhao, Y.M.; Zhang, N. Creep Behavior of Epoxy-Bonded Anchor System. *Int. J. Rock Mech. Min. Sci.* **2014**, *67*, 96–103. [CrossRef]
10. Kim, N. Performance of Tension and Compression Anchors in Weathered Soil. *J. Geotech. Geoenviron. Eng.* **2003**, *129*, 1138–1150. [CrossRef]
11. Wu, G.J.; Chen, W.Z.; Jia, S.P.; Yang, J.P. Shear Creep Experiments for Anchorage Interface Mechanic and Nonlinear Rheological Model of Rocks. *Chin. J. Rock Mech. Eng.* **2010**, *29*, 520–527. (In Chinese)
12. Chen, C.F.; Liu, J.B.; Xu, Y.L.; Zhang, B.G. Tests on Shearing Creep of Anchor-Soil Interface and Its Empirical Model. *Chin. J. Geot. Eng.* **2016**, *38*, 1762–1768. (In Chinese) [CrossRef]
13. Jiang, S.H.; Li, D.Q.; Zhang, L.M.; Zhou, C.-B. Time-Dependent System Reliability of Anchored Rock Slopes Considering Rock Bolt Corrosion Effect. *Eng. Geol.* **2014**, *175*, 1–8. [CrossRef]
14. Montero-Cubillo, N.S.; Galindo-Aires, R.A.; Serrano-Gonzalez, A.; Olalla-Maranon, C.; Simic-Sureda, F.D. Analytical Model of an Anchored Wall in Creep Soils. *Int. J. Geomech.* **2020**, *20*, 04020027. [CrossRef]
15. Shi, K.Y.; Wu, X.P.; Liu, Z.; Dai, S.L. Coupled Calculation Model for Anchoring Force Loss in a Slope Reinforced by a Frame Beam and Anchor Cables. *Eng. Geol.* **2019**, *260*, 105245. [CrossRef]
16. Wang, J.; Liu, J.; Cao, P.; Liang, Q.; Duan, J. Coupled Creep Characteristics of Anchor Structures and Soils under Chemical Corrosion. *Indian Geotech. J.* **2017**, *47*, 521–528. [CrossRef]
17. Wang, J.; Liang, Q.; Duan, J. The Creep Model of the Anchorage Structure and the Time-Dependent Reliability Analysis. *Front. Earth Sci.* **2020**, *8*, 44. [CrossRef]
18. Zhang, C.C.; Zhu, H.H.; Xu, Q.; Shi, B.; Mei, G.X. Time-Dependent Pullout Behavior of Glass Fiber Reinforced Polymer (Gfrp) Soil Nail in Sand. *Can. Geotech. J.* **2015**, *52*, 671–681. [CrossRef]
19. Fang, C.Q.; Shen, X.Y.; He, K.; Yin, C.; Li, S.S.; Chen, X.L.; Sun, H.Y. Application of Fractional Calculus Methods to Viscoelastic Behaviours of Solid Propellants. *Philos. Trans. R. Soc. A* **2020**, *378*, 20190291. [CrossRef]
20. Schiessel, H.; Metzler, R.; Blumen, A.; Nonnenmacher, T.F. Generalized Viscoelastic Models: Their Fractional Equations with Solutions. *J. Phys. A-Math. Gen.* **1995**, *28*, 6567–6584. [CrossRef]
21. Adolfsson, K.; Enelund, M.; Olsson, P. On the Fractional Order Model of Viscoelasticity. *Mech. Time-Depend. Mater.* **2005**, *9*, 15–34. [CrossRef]
22. Cai, W.; Chen, W.; Xu, W.X. Characterizing the Creep of Viscoelastic Materials by Fractal Derivative Models. *Int. J. Non-Linear Mech.* **2016**, *87*, 58–63. [CrossRef]
23. Liu, F.; Zhuang, P.; Turner, I.; Burrage, K.; Anh, V. A New Fractional Finite Volume Method for Solving the Fractional Diffusion Equation. *Appl. Math. Model.* **2014**, *38*, 3871–3878. [CrossRef]
24. Qu, H.D.; Liu, X. A Numerical Method for Solving Fractional Differential Equations by Using Neural Network. *Adv. Math. Phys.* **2015**, *2015*, 439526. [CrossRef]
25. Pindza, E.; Owolabi, K.M. Fourier Spectral Method for Higher Order Space Fractional Reaction-Diffusion Equations. *Commun. Nonlinear Sci. Numer. Simul.* **2016**, *40*, 112–128. [CrossRef]
26. Bueno-Orovio, A.; Kay, D.; Burrage, K. Fourier Spectral Methods for Fractional-in-Space Reaction-Diffusion Equations. *BIT Numer. Math.* **2014**, *54*, 937–954. [CrossRef]
27. Hosseini, V.R.; Chen, W.; Avazzadeh, Z. Numerical Solution of Fractional Telegraph Equation by Using Radial Basis Functions. *Eng. Anal. Boundary Elem.* **2014**, *38*, 31–39. [CrossRef]
28. Khodabakhshi, N.; Vaezpour, S.M.; Baleanu, D. Numerical Solutions of the Initial Value Problem for Fractional Differential Equations by Modification of the Adomian Decomposition Method. *Fract. Calc. Appl. Anal.* **2014**, *17*, 382–400. [CrossRef]
29. Kim, M.H.; Ri, G.C.; Hyong-Chol, O. Operational Method for Solving Multi-Term Fractional Differential Equations with the Generalized Fractional Derivatives. *Fract. Calc. Appl. Anal.* **2014**, *17*, 79–95. [CrossRef]
30. Majak, J.; Shvartsman, B.; Pohlak, M.; Karjust, K.; Eerme, M.; Tungel, E. Solution of Fractional Order Differential Equation by the Haar Wavelet Method. In Proceedings of the International Conference on Numerical Analysis and Applied Mathematics (ICNAAM), Rhodes, Greece, 23–29 September 2015. [CrossRef]
31. Wang, Q.B.; Zhang, C.; Wang, H.; Wen, X.K.; Shi, Z.Y.; Lv, R.S.; Wang, T.T. Study of Coupling Effect between Anchorage Force Loss of Prestressed Anchor Cable and Rock and Soil Creep. *Rock Soil Mech.* **2014**, *35*, 2150–2156, 2162. (In Chinese) [CrossRef]
32. Wang, G.F.; Li, Q.; Lu, L.; Cao, Z.L. A Coupled Model Research of Anchor Prestress Loss Considering the Relaxation Characteristics of Anchor. *Chin. J. Undergr. Space Eng.* **2017**, *13*, 1585–1591. (In Chinese)
33. Shi, K.Y.; Wu, X.P.; Tian, Y.R.; Xie, X.T. Analysis of Re-Tensioning Time of Anchor Cable Based on New Prestress Loss Model. *Mathematics* **2021**, *9*, 1094. [CrossRef]
34. Xu, Y.Q.; Deng, S.Y.; Ge, Q. Prediction Models for Short-Term and Long-Term Pre-Stress Loss of Anchor Cable. *Rock Soil Mech.* **2020**, *41*, 1663–1669. [CrossRef]
35. Chen, J.; Wang, D.; Feng, C.L. Analysis of Locking Value of Anchor Cable in Pile Anchor Supporting Structure. *Adv. Mater. Res.* **2014**, *838–841*, 203–208. [CrossRef]
36. Wang, X.X.; Chen, Z.H.; Liu, H.B.; Yu, Y.J. Experimental Study on Stress Relaxation Properties of Structural Cables. *Constr. Build. Mater.* **2018**, *175*, 777–789. [CrossRef]
37. Nanni, A.; Bakis, C.E.; O'Neil, E.F.; Dixon, T.O. Short-Term Sustained Loading of Frp Tendonanchor Systems. *Constr. Build. Mater.* **1996**, *10*, 255–266. [CrossRef]

38. Li, J.H.; Wang, Y.; Deng, J.; Jia, Y.H. Experimental Study on the Flexural Behaviour of Notched Steel Beams Strengthened by Prestressed Cfrp Plate with an End Plate Anchorage System. *Eng. Struct.* **2018**, *171*, 29–39. [CrossRef]
39. Wu, L.Z.; Li, B.; Huang, R.Q.; Sun, P. Experimental Study and Modeling of Shear Rheology in Sandstone with Non-Persistent Joints. *Eng. Geol.* **2017**, *222*, 201–211. [CrossRef]
40. Zhao, Y.L.; Wang, Y.X.; Wang, W.J.; Wan, W.; Tang, J.Z. Modeling of Non-Linear Rheological Behavior of Hard Rock Using Triaxial Rheological Experiment. *Int. J. Rock Mech. Min. Sci.* **2017**, *93*, 66–75. [CrossRef]
41. He, Z.L.; Zhu, Z.D.; Ni, X.H.; Li, Z.J. Shear Creep Tests and Creep Constitutive Model of Marble with Structural Plane. *Eur. J. Environ. Civ. Eng.* **2019**, *23*, 1275–1293. [CrossRef]
42. Zhang, S.G.; Liu, W.B.; Lv, H.M. Creep Energy Damage Model of Rock Graded Loading. *Results Phys.* **2019**, *12*, 1119–1125. [CrossRef]
43. Liu, J.F.; Wang, L.; Pei, J.L.; Zheng, L.; Bian, Y. Experimental Study on Creep Deformation and Long-Term Strength of Unloading-Fractured Marble. *Eur. J. Environ. Civ. Eng.* **2015**, *19*, S97–S107. [CrossRef]
44. Liu, H.Z.; Xie, H.Q.; He, J.D.; Xiao, M.L.; Zhuo, L. Nonlinear Creep Damage Constitutive Model for Soft Rocks. *Mech. Time-Depend. Mater.* **2017**, *21*, 73–96. [CrossRef]
45. Liu, Y.; Liu, C.W.; Kang, Y.M.; Wang, D.; Ye, D.Y. Experimental Research on Creep Properties of Limestone under Fluid-Solid Coupling. *Environ. Earth Sci.* **2015**, *73*, 7011–7018. [CrossRef]
46. Krankel, T.; Lowke, D.; Gehlen, C. Prediction of the Creep Behaviour of Bonded Anchors until Failure—A Rheological Approach. *Constr. Build. Mater.* **2015**, *75*, 458–464. [CrossRef]
47. Chen, G.Q.; Chen, T.; Chen, Y.; Huang, R.Q.; Liu, M. A New Method of Predicting the Prestress Variations in Anchored Cables with Excavation Unloading Destruction. *Eng. Geol.* **2018**, *241*, 109–120. [CrossRef]
48. Prieto-Munoz, P.A.; Yin, H.M.; Testa, R.B. Mechanics of an Adhesive Anchor System Subjected to a Pullout Load. Ii: Viscoelastic Analysis. *J. Struct. Eng.* **2014**, *140*, 04013053.1–04013053.13. [CrossRef]
49. He, Z.Y.; An, X. Prestress Loss Model and Experimental Study of Anchor Cables in Soft Soil Area. *Mater. Sci. Inf. Technol.* **2012**, *433–440*(Pts 1–8), 2769–2773. [CrossRef]
50. Xu, H.F.; Wang, F.J.; Cheng, X.X. Pullout Creep Properties of Grouted Soil Anchors. *J. Cent. South Univ. Technol.* **2007**, *14*, 474–477. [CrossRef]
51. Chen, A.M.; Gu, J.C.; Shen, J.; Ming, Z.Q. Model Testing Research on the Variation of Tension Force of Anchor Cable with Time in Reinforcement of Soft Rocks. *Chin. J. Rock Mech. Eng.* **2002**, *21*, 251–256. (In Chinese)
52. Tang, M.X. Test Study on Anchorage Force of Prestress Anchor Cables for Foundation Pit. *Chin. J. Rock Mech. Eng.* **2007**, *26*, 1158–1163. (In Chinese)